CIVIL ENGINEERING JOURNAL

Article no. 34

THE CIVIL ENGINEERING JOURNAL 4-2025

EXPERIMENTAL STUDY ON MECHANICAL PROPERTIES, FAILURE, AND DILATANCY BEHAVIOUR OF HIGH- AND ULTRA- HIGH -STRENGTH CONCRETE UNDER TRIAXIAL COMPRESSIVE STRESS

Mingyu Feng [1] and Yanbin Zhang [2]

1. *Hebei University of Engineering, Handan 056038, China; myufeng@163.com*
2. *China architecture design & research group, Beijing 100044, China; yanbinzhang1236@163.com*

Received: *26.09.2024*
Received in revised form: *11.04.2025*
Accepted: *24.11.2025*

ABSTRACT

To study the mechanical properties of high- and ultra-high-strength concrete, the conventional triaxial tests were carried out on four types of concrete with uniaxial strengths of 67.01, 109.34, 140.65, and 159.61 MPa under six levels of confining pressure. The influence on the failure mode, strength, deformability, and dilation properties of four kinds of concrete with different strengths by the confining pressure was studied. The test results show that: the cracks generated in high strength concrete always bypassed the coarse aggregate, and the percentages of aggregates bypassed were 85.7% and 70.5%, while in ultra-high-strength concrete, the cracks mainly passed through the coarse aggregate, fewer cracks bypass the aggregate, and the percentages of bypassed aggregate is 28.7% and 32.8%, respectively. With increasing confining pressure, the peak stress and stress of dilatancy onset of four types of concrete increase, and the corresponding strain at peak stress and dilatancy onset mount approximately linearly. The enhancement of the confining pressure on the peak stress, stress of dilatancy onset, strain at the peak stress and dilatancy onset in a negative relation to the uniaxial compressive strength of concrete. The peak volumetric strain of concrete increases as the confining pressure mounts. Under the same condition of confining pressure, the lower the uniaxial compressive strength is, the higher the volumetric strain is. The parameters were modified to make the volumetric model more suitable to describe the change law of volume for high- and ultra-high-strength concrete with a wider range of confining pressure levels. The failure envelopes of four kinds of concrete under uniaxial and triaxial stress states were obtained by using the nonlinear Mohr-Coulomb criterion.

KEYWORDS

High- and ultra-high-strength concrete, Triaxial compression, Failure modes, Peak stress, Dilatancy behaviour, Volumetric model

INTRODUCTION

As one of the most commonly used building materials, concrete is widely used in various structures. In actual concrete members, concrete is usually in a state of multiaxial stress. Since the 1930s, some researchers have paid attention to the law of strength and deformation of concrete under multiaxial stress. Richart et al. [1] conducted comprehensive studies on the failure of normal

strength concrete (NSC) under uniaxial, biaxial and triaxial compressive stresses and found that the compressive strength and deformability of NSC gradually had been improved by increasing of confining pressure. Afterwards, many scholars [2-5] also conducted a lot of studies on the mechanical properties of NSC under triaxial compression, and the results all showed that the confining pressure has a great influence on the compressive strength and deformability of NSC.

Since the 1990s, with the wide application of high-strength concrete (HSC), many scholars have begun to study the mechanical properties of HSC under multiaxial stress states. Xie et al. [6] conducted conventional triaxial tests on three types of HSC containing silica fume and the quartzite aggregates whose size are less than 14 mm. The results showed that the compression strength, residual compression strength and the deformability of HSC were significantly improved, but they were still less than those of NSC. Song and He [7, 8] conducted biaxial and triaxial compression tests on high strength concrete with the uniaxial compressive strength of 60 MPa. They studied its strength and deformation properties under different confining pressure levels. To determine the failure surface of high-strength concrete, a series of triaxial compression tests were carried out by Ansari and Li [9] on three types of concrete with uniaxial strength of 47, 71 and 107 MPa, respectively. According to the test results, the empirical formula between compression strength of concrete and confining pressure was obtained, as well as failure surfaces in principal stress space were established.

With the progress of technology on cement-based materials, the concrete was produced with uniaxial compressive strength exceeding 120 MPa, which can be called ultra-high-strength concrete (UHSC) and ultra-high-performance concrete (UHPC), and have widely been used in super tall buildings, offshore concrete structures, and long-span concrete structures. In the existing literature, most of the analyses were based on the mechanical properties of NSC and HSC under triaxial stress. While for UHSC, scholars frequently pay more attention to its properties under the uniaxial compression [10, 11], tensile conditions [12] and biaxial compression states [13, 14]. Similar to NSC and HSC, UHSC is usually under the triaxial stress states in the structure. Wang et al. [15] conducted a series of tests on UHSC without coarse aggregate and UHPC with steel fibers under uniaxial and triaxial compression. The result showed that the compression strength and deformability all increased as the confining pressure increased. The confining pressure has a slightly lower enhancement on the compressive strength of UHPC compared with UHSC. However, the failure of the UHPC was obviously lagging that of the UHSC because of the restraint effect of steel the fiber and confining pressure, showing more excellent ductility.

Although there have been certain studies on the mechanical properties of UHSC under triaxial stress to date, there are still few systematic quantitative studies on high-strength and ultra-high-strength concrete containing coarse aggregates. Besides, with the wide use of computer technology in various fields, various numerical methods have been applied to the design and analysis of building structures. The accuracy of the constitutive model of building structure materials has a marked impact on the accuracy of the prediction results of numerical methods. Most constitutive models were founded according to the test data of NSC and HSC in the past. Whether they could be applied in UHSC is still debatable. Therefore, obtaining a more accurate constitutive model and establishing corresponding failure criteria of UHSC to predict its performance under multiaxial stress is of great significance to fully understand and exert its superior mechanical properties [16-18].

In this paper, four kinds of concrete with different strengths were prepared, containing the same basalt coarse aggregate, and the uniaxial compression test and the conventional triaxial compression test under confining pressure of 5, 10, 20, 40, and 70 MPa were carried out, respectively. The mechanical properties of concrete under uniaxial and triaxial stress states were studied, and the peak stress, corresponding strain at the point of peak stress, stress and corresponding strain of dilatancy onset, as well as the failure modes of four concretes were compared at the same time. Based on the test data, the failure envelopes were obtained by using the nonlinear Mohr-Coulomb criterion, which was used to describe the mechanical properties of concrete under triaxial stress states.

MATHERIALS AND METHODS

Four kinds of concrete are designed for testing, two of which are HSC. The water/binder ratios are 0.4 and 0.3, respectively, represented by HSC-1 and HSC-2; The other two are UHSC, and the water/binder ratios are 0.25 and 0.18, respectively, which are represented by UHSC-1 and UHSC-2.

MATERIALS AND MIXTURE PROPOTION

The constituent materials used for all concrete mixture proportions in this study included cement, quartz sand, basalt coarse aggregate, and water. Additionally, the quartz powder and water reducer were used to prepare HSC-2, UHSC-1, and UHSC-2; the FAQ defoamer was used to prepare HSC-1 and HSC-2; the silica fume was used to prepare UHSC-1 and UHSC-2. During the preparation process, the quartz sand and coarse aggregate are both saturated-surface-dry states. The mixture proportions are as follows in Table 1.

Tab. 1 - The mixture proportions (kg/m^3)

Materials	HSC-1	HSC-2	UHSC-1	UHSC-2
Portland Cement P·O52.5R	480	550	440	470.
Quartz sand (0.16-0.63 mm)	590	450	490	470
Basalt coarse aggregate (3-10 mm)	1200	1200	1200	1200
Water	190	165	130	100
Quartz powder (<80 μm)	–	120	120	125
Silica fume (0.1 μm)	–	–	90	95
FAQ defoamer	0.85	0.75	–	–
Water reducer	–	3.75	4.50	16.50

Sample preparation

During sample preparation, firstly, put the materials described in Table 1 into a horizontal mixer and mix them evenly, and pour into the molds of 280 mm × 240 mm × 200 mm, then use the vibrating screed to eliminate large air pockets and bubbles in the concretes. The surface of the vibrated concrete was covered with plastic wrap and placed them into the standard curing room. The molds were removed after 48 hours. Before the test, the concretes were in the curing room for more than 519 days, and their mechanical properties can be considered stable. Before the test, the cylindrical core samples with the size of about Φ 49×180 mm were taken from the concrete blocks by drill machine, a cutting machine and a double-end grinder were used to process the samples into Φ 49×120 mm cylindrical samples. The unevenness of the end face is no more than 0.1 mm, and the error of diameter and height is no more than 0.4 mm.

Test equipment and test methods

The XTR01 high-pressure triaxial test machine was used to carry out experiments, which is mechanically loaded in the axial direction, with a maximum load of 2000 kN, and hydraulically loaded in the lateral direction, with a maximum confining pressure of 100MPa. During the test, the actual axial pressure stress of the sample is $\sigma_c = q + p$, where p is confining pressure, and q is differential stress. The schematic diagram of the force on the sample is shown in Figure 1.

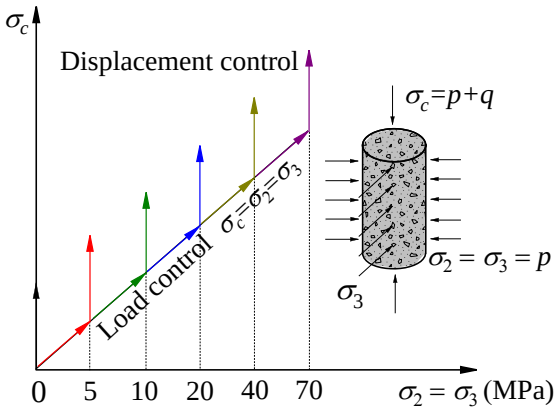

Fig.1 – Sample force diagram and load path

The symbols of stress and strain involved in this paper are positive for compression and negative for tension. ε_r represents the average radial strain, and its expression is $\varepsilon_r = (\varepsilon_2 + \varepsilon_3)/2$, where ε_2 and ε_3 represent the two radial strains respectively in the perpendicular direction at the same height of the sample; ε_c represents the axial strain. Figure 2 is the installation of extensometers.

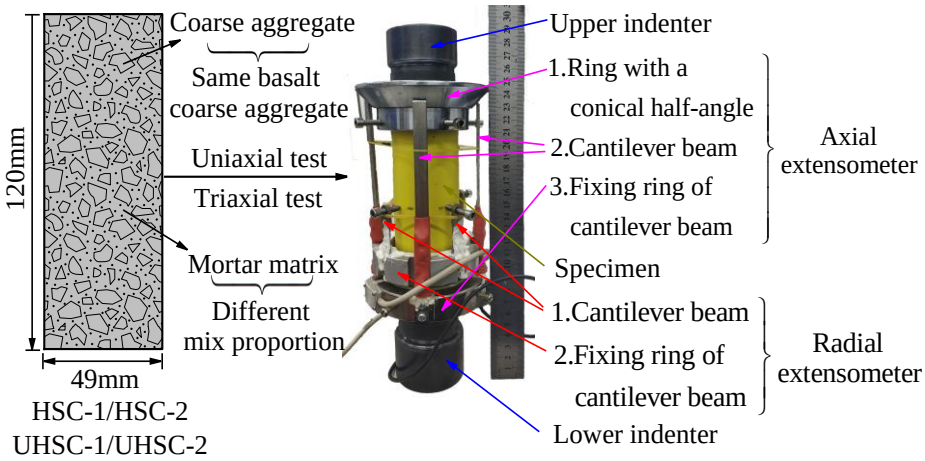

Fig.2 – Installation of extensometers

In the initial phase of the experiment, the sample is firstly preloaded, so that upper indenter could be mildly adjusted in position with the end face of the sample. In this way, the lower and the upper end surfaces of the indenter are in completely contact with the upper end surface of the sample and the lower end surface of the plunger, respectively, so as to avoid eccentric force on the sample. In the uniaxial compression test, the axial displacement is applied with the constant rate of 0.001 mm/s after preloading. In triaxial test, the lateral confining pressure is applied with the rate of 0.1 MPa/s after completion of preloading. When the confining pressure reaches the design values, the lateral confining pressure was kept constant for about 5 minutes, and then the axial displacement is applied monotonously with the rate of 0.001 mm/s. Two samples of the same type are used for the test under each confining pressure.

TEST RESULTS

Figure 3 shows the differential stress-strain curves of four concretes under various confining pressures. For the same type of samples, the straight-line sections of curves have an almost constant slope before the peak point, indicating that the elastic modulus of the four kinds of concrete is not greatly influenced by confining pressure.

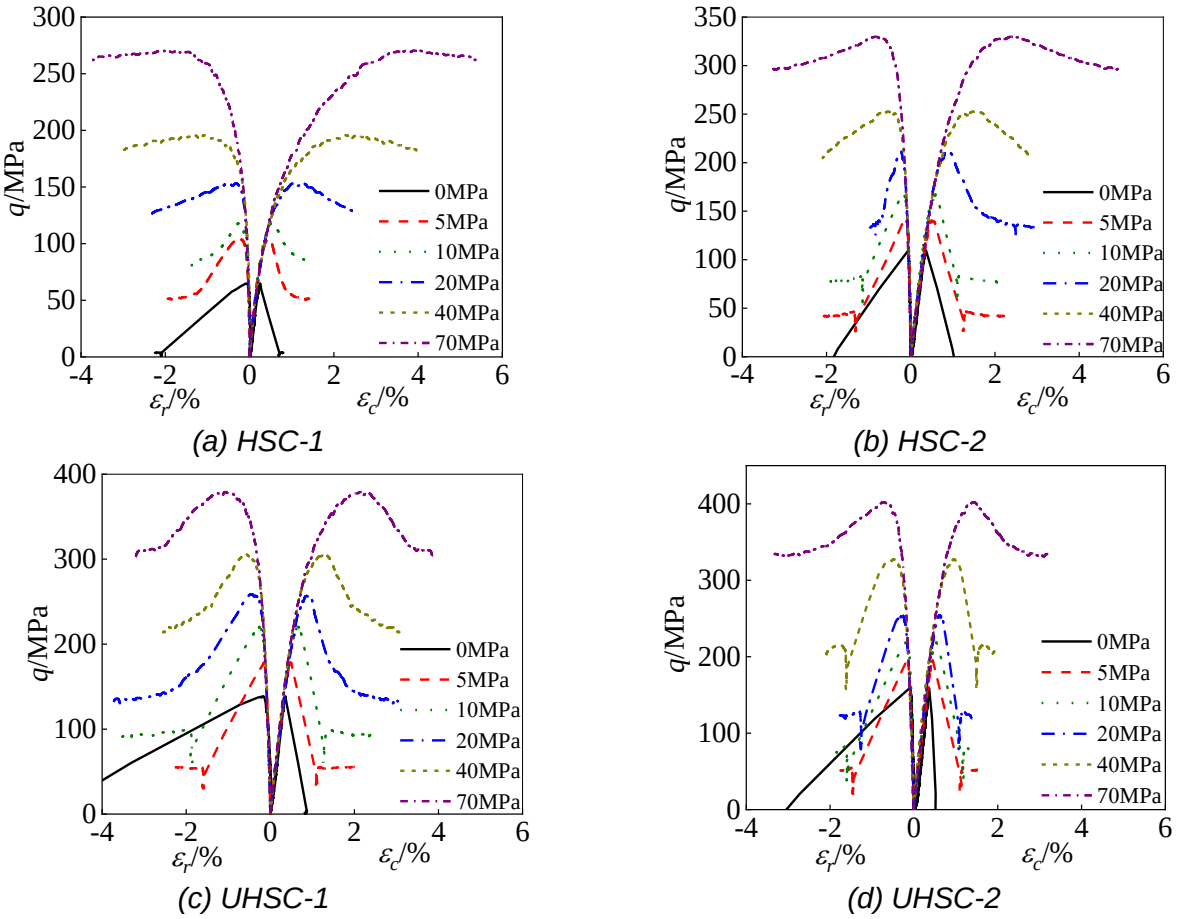

Fig.3 – Differential stress-strain curves of concrete under different confining pressures

At low confining pressure, the differential stress of all samples increases linearly with the increase of strain within a large stress range before the peak point. The deviatoric stress falls faster after passing the peak point with the deformation suddenly increases, which is maybe caused by the insufficient stiffness of the testing machine. Under the high confining pressure, the curve rises linearly just in a small range of stress, and the differential stress falls slowly after the peak point. At the same time, under the same confining pressure, the higher the uniaxial strength of concrete, the sharper the peak of the curve and the faster the stress drop after the peak, showing more brittle characteristics. The mean values of peak stress and corresponding strain at peak stress of four kinds of concrete under six levels of confining pressures are listed in Table 2. $\sigma_{cc}$and ε_{cc} represent the peak stress and corresponding strain at peak stress of concrete, respectively.

Tab. 2 - Triaxial compression test results

p/MPa	HSC-1		HSC-2		UHSC-1		UHSC-2	
	σ_{cc}/MPa	ε_{cc}/%	σ_{cc}/MPa	ε_{cc}/%	σ_{cc}/MPa	ε_{cc}/%	σ_{cc}/MPa	ε_{cc}/%
0	67.01	0.285	109.34	0.322	140.65	0.363	159.61	0.382
5	111.64	0.482	160.12	0.498	188.14	0.512	203.53	0.444
10	129.74	0.559	181.25	0.607	225.16	0.641	234.36	0.536
20	170.98	1.135	234.48	0.847	281.24	0.892	289.63	0.610
40	235.35	2.268	306.46	1.495	347.81	1.273	367.07	0.977
70	345.18	3.916	395.35	2.435	447.62	2.109	471.04	1.427

Figure 4 shows the failure modes of samples in triaxial compressive test. It is found that as the confining pressure rises, the failure modes of the same samples show the trend that splitting failure at uniaxial compression, an oblique shear failure occurs at low confining pressure, while to extrusion flow failure appears at high confining pressures.

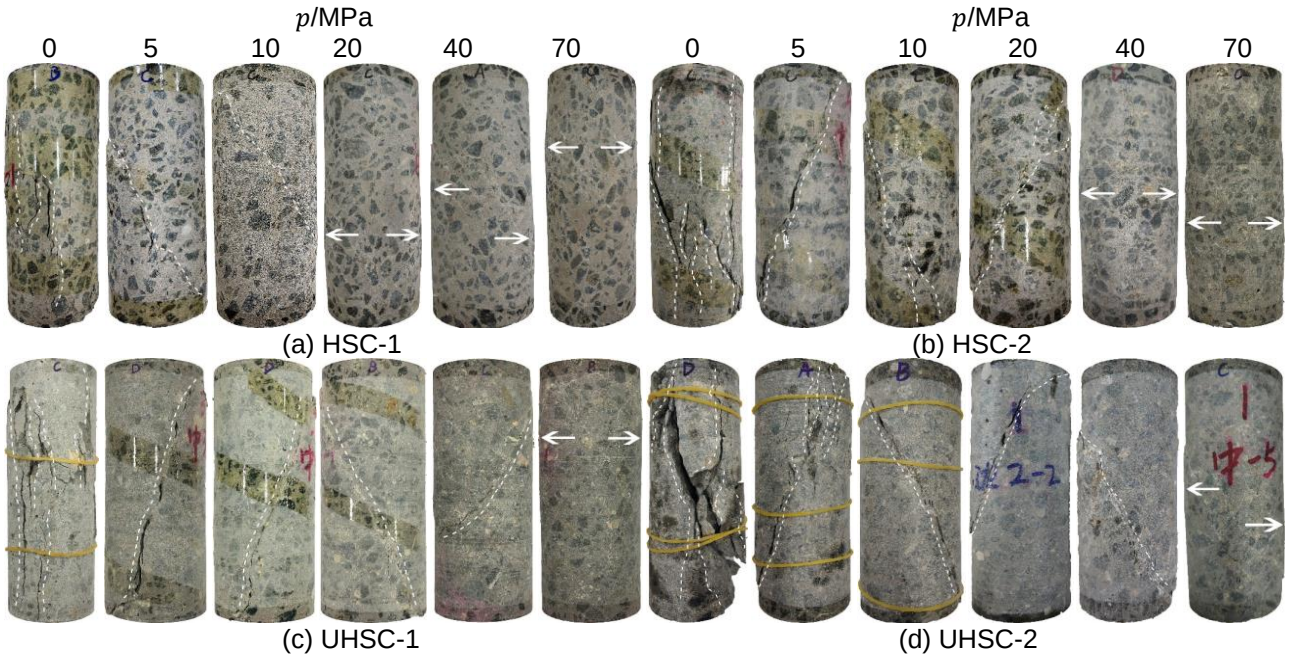

Fig.4 – Failure modes of samples at different confining pressures

The failure modes of the four kinds of concrete are all oblique shear failure when the confining pressure is 5, 10 MPa, and a diagonal crack appears on the surface of the samples. When the confining pressure is 20 MPa, the failure mode of HSC-1 is extrusion flow failure, many small irregular cracks are formed on the surface of the middle part of the sample, and evident bulging occurs, while the failure modes of the other three kinds of concrete are still oblique shear failure. When the confining pressure is 40MPa, the failure modes of HSC-1 and HSC-2 are both extrusion flow failure, and there are many small irregular cracks in the middle of the sample with obvious bulging, while the failure modes of UHSC-1 and UHSC-2 are still oblique shear failure, while diagonal shear crack is less obvious than that of low confining pressure. When the confining pressure is 70 MPa, the failure modes of the four samples are all extrusion flow failure. The reason for the different failure modes of the same sample is that the cracks generated in the sample are not easy to expand because of confining pressure. A through crack can be generated at a low confining pressure level, which makes the bearing capacity of the sample drop suddenly, and the sample shows oblique shear failure; while under the high stress level, the confining pressure significantly inhibits the crack propagation; the cracks in the sample gradually increase, but it is not easy to connect, which makes the axial stress of the sample decline slowly, and finally forms the extrusion flow failure.

Figure 5 summarizes the trend of cracks on the surface of samples after the failure. The aggregates indicated by the red arrow are the aggregates bypassed when the crack propagates, and the aggregates indicated by the green arrow are the aggregates traversed by the propagation of the cracks.

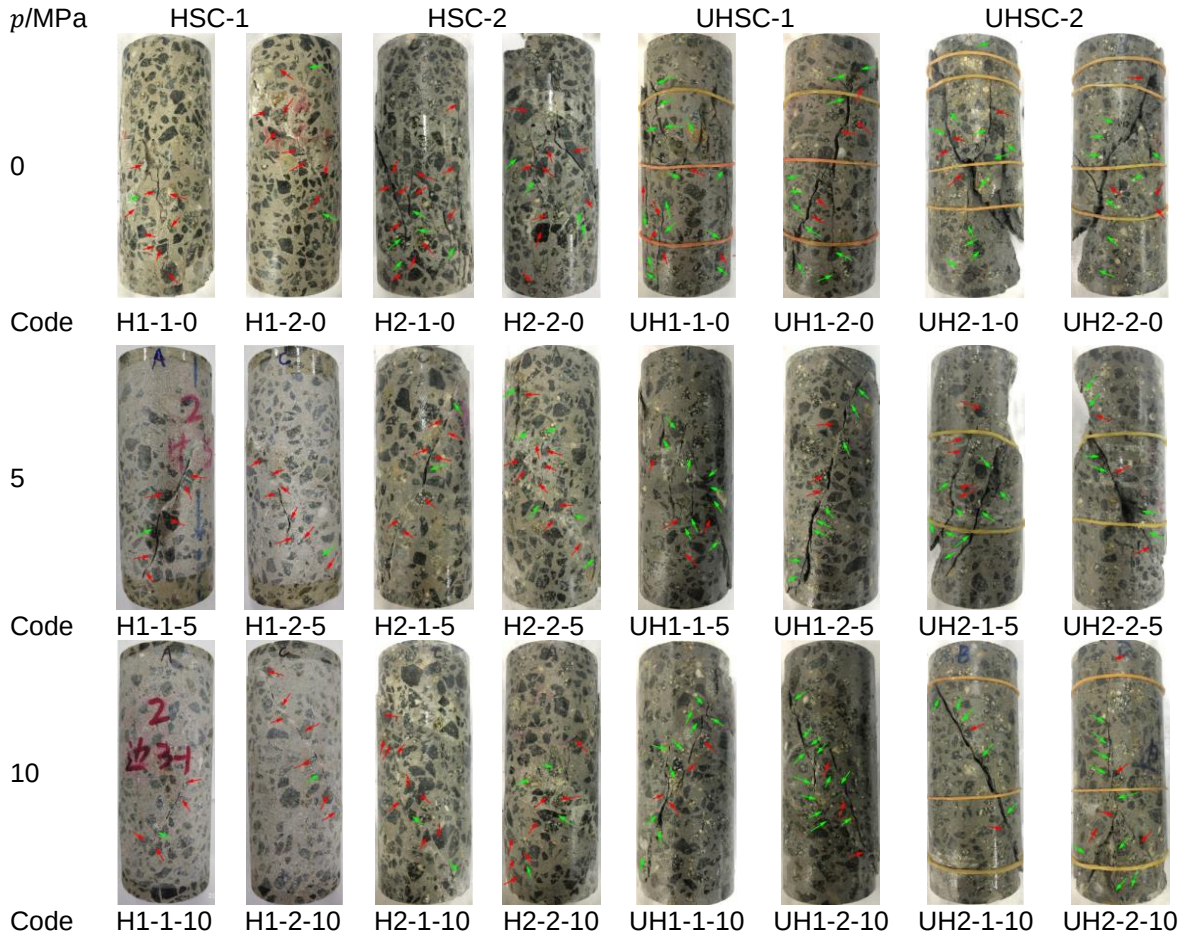

Fig.5 – Detailed view of the crack path on the surface of the concrete

Table 3 shows the number of coarse aggregates that are bypassed and traversed by the cracks, where I and T represent that crack bypassing aggregate and transferring aggregate, respectively.

Tab. 3: Statistics of the number of cracks passing through aggregate and bypassing aggregate

Code	I	T	Code	I	T	Code	I	T	Code	I	T
H1-1-0	9	1	H2-1-0	12	5	UH1-1-0	6	14	UH2-1-0	4	11
H1-2-0	8	2	H2-2-0	9	4	UH1-2-0	5	10	UH2-2-0	4	8
H1-1-5	6	1	H2-1-5	7	2	UH1-1-5	4	8	UH2-1-5	5	8
H1-2-5	8	1	H2-2-5	10	6	UH1-2-5	3	8	UH2-2-5	3	6
H1-1-10	4	1	H2-1-10	9	2	UH1-1-10	4	10	UH2-1-10	2	5
H1-2-10	7	1	H2-2-10	8	4	UH1-2-10	3	12	UH2-2-10	5	9
Total	42	7	Total	55	23	Total	25	62	Total	23	47
(%)	85.7	14.3	(%)	70.5	29.5	(%)	28.7	71.3	(%)	32.8	67.2

As can be found from Figure 5 and Table 3 that for the HSC-1 and HSC-2, no matter which failure modes the samples are, the cracks mostly choose to bypass the aggregate, and the cracks mainly occur in the matrix or extend along the interface between the mortar and aggregate, the paths of cracks are relatively tortuous and irregular; the fracture is mainly caused by the damage of the mortar matrix. This because the matrix strength is lower than coarse aggregate strength, according

to the principle of minimum energy, the crack always selects the path of less energy consumption to expand, and the aggregate hinders the expansion of cracks in concrete, which makes the cracks only propagate in the area without coarse aggregate. This failure form can be called intergranular failure [19]. For UHSC-1 and UHSC-2, whether in uniaxial compression or triaxial compression, the cracks generated by the failure mostly choose to pass through the coarse aggregates when they expand to the aggregates, forming a relatively continuous and smooth crack path. The failure of the concrete is mainly caused by joint damage of matrix and aggregate, this is mainly because that the strength of matrix has little different from coarse aggregate in the UHSC, and the hindrance of the aggregate on the crack propagation is not obvious. This failure pattern was a transgranular failure [19].

According to the different forms of failure modes, the three failure modes are divided into three types, which can be called type I, II and III, respectively. To analyze the influence of confining pressure on the failure modes of concrete, the confining pressure was normalized by uniaxial compression strength. The distribution of failure modes in the coordinate plane of confining pressure level and uniaxial strength was shown in Figure 6. The relationship between failure mode and confining pressure level of UHSC in the text of Zhou [16]is referred to in the figure. The dotted line was the boundary of different failure types.

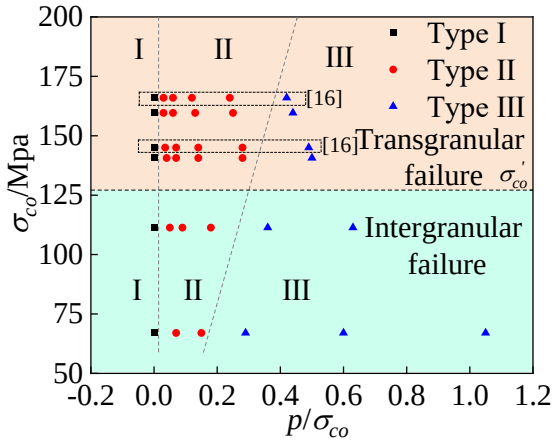

Fig.6 – Distribution of failure modes of concrete under different confining pressure levels

From Figure 6, it can be found that the uniaxial compression strength has little effect on the failure mode of concrete. Four kinds of concrete showed vertical splitting failure under uniaxial compression. However, as the strength increases, the larger confining pressure level was required for the transformation from oblique shear failure to extrusion flow failure. Through the analysis of the relationship between the path of crack propagation and the position of aggregate, there is a critical strength σ_{co}' exists, when $\sigma_{co} \leq \sigma_{co}'$, the failure morphology of concrete is an intergranular failure, and when $\sigma_{co} > \sigma_{co}'$, the failure morphology of concrete is a transgranular failure, the value of σ_{co}' is related to the strength of coarse aggregate in concrete, the value range in this article is 109.34 MPa $\leq \sigma_{co}' <$ 140.65 MPa. Figure 7 shows a schematic diagram of the failure morphologies of the intergranular failure and the transgranular failure in the three failure modes.

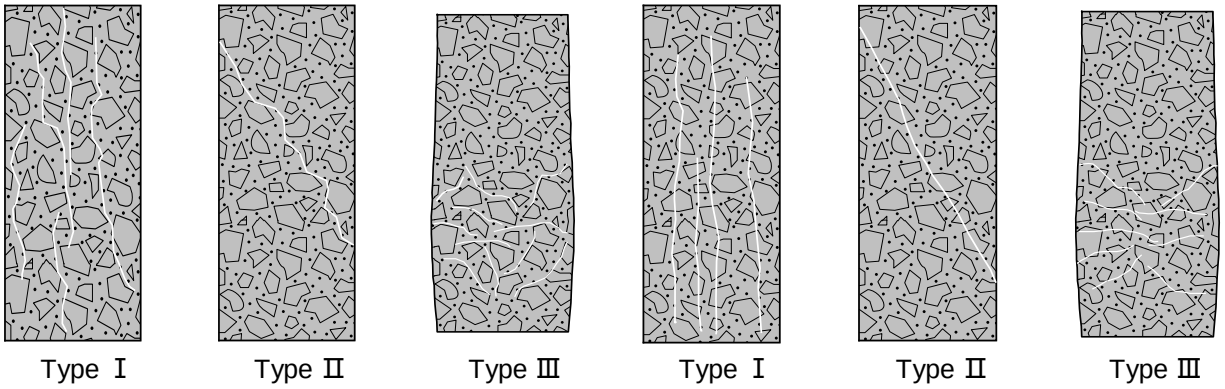

(a) Intergranular failure *(b) Transgranular failure*

Fig.7 – Schematic diagram of failure morphologies

DISCUSSION AND ANALYSIS

Peak stress and axial strain at peak stress

The peak stress and corresponding strain at peak stress of four kinds of concrete were normalized by uniaxial compression strength and corresponding uniaxial strain at peak stress. The relationship of σ_{cc}/σ_{co}-p/σ_{co} and $\varepsilon_{cc}/\varepsilon_{co}$-$p/\sigma_{co}$ were drawn. To compare the influence on the compression strength and axial deformability of four concretes by the confining pressure level, the experimental data were fitted by the Eqs. (1) and (2). The corresponding fitting curves were shown in Figures 8 and 9.

$$\frac{\sigma_{cc}}{\sigma_{co}} = \sqrt{1 + k\frac{p}{\sigma_{co}}} \tag{1}$$

$$\frac{\varepsilon_{cc}}{\varepsilon_{co}} = 1 + b\frac{p}{\sigma_{co}} \tag{2}$$

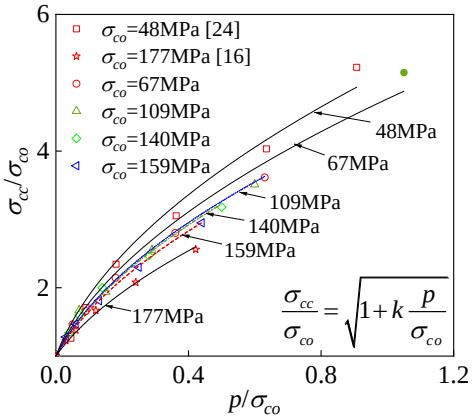

Fig.8 – Relationship between σ_{cc}/σ_{co}-p/σ_{co}

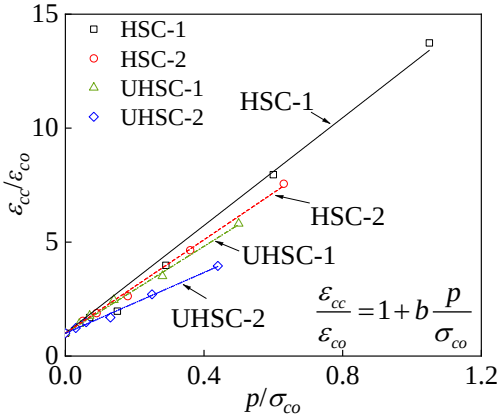

Fig.9 – Relationship between $\varepsilon_{cc}/\varepsilon_{co}$-$p/\sigma_{co}$

where k and b are the parameters representing the rate of compression strength growth and axial strain growth with confining pressure. The values of parameters k and b in relation to the type of concrete [16, 24] and are shown in Table 4, where R^2 refers to the coefficient of determination.

Tab.4: The fitting parameter values for curves in Figures 8 and 9

Type	Imran [24]		HSC-1		HSC-2		UHSC-1		UHSC-2		Zhou [16]	
Parameters	k	b	k	b	k	b	k	b	k	b	k	b
Value	25.75	-	24.11	11.82	19.32	10.26	18.81	9.54	17.53	6.67	13.64	-
R^2	0.98	-	0.98	0.99	0.99	0.99	0.99	0.99	0.98	0.98	0.96	-

As can be seen from Figures 8 and 9 that the peak stress σ_{cc} gradually increases nonlinearly as the confining pressure rises, while the strain at peak stress ε_{cc} increases approximately linearly as confining pressure increases. Confining pressure has a conducive influence on improving the strength and deformability of concrete. It also can be seen that whether it is HSC or UHSC, with the increase in confining pressure, the lower the σ_{co} of concrete, the higher the growth rate of the σ_{cc} of concrete, which shows that the enhancement on the compression strength of the relatively low-strength concrete by confining pressure is greater than that of the relatively high-strength concrete. Similarly, the lower the σ_{co} of concrete, the higher the growth rate of axial deformation with confining pressure, which indicates that the enhancement on the deformability of the relatively low-strength concrete by confining pressure is greater than that of the relatively high-strength concrete. In summary, the enhancement effect on the strength and axial deformation of concrete in triaxial compression test are all in negative relation to the uniaxial compressive strength.

Stress and axial strain of dilatancy onset

Figures 10 and 11 show the normalized relation between the stress, axial strain of dilatancy onset and the confining pressure level, respectively

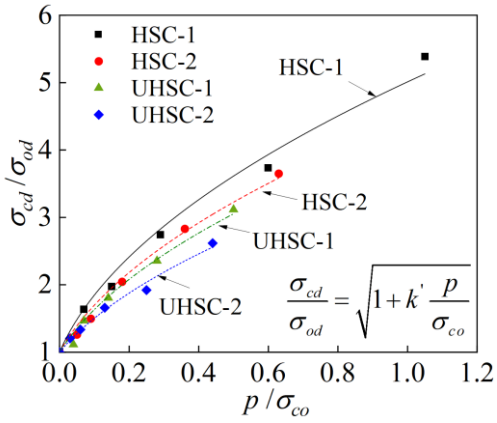

Fig.10 – Relationship between p/σ_{co} and σ_{cd}/σ_{od}

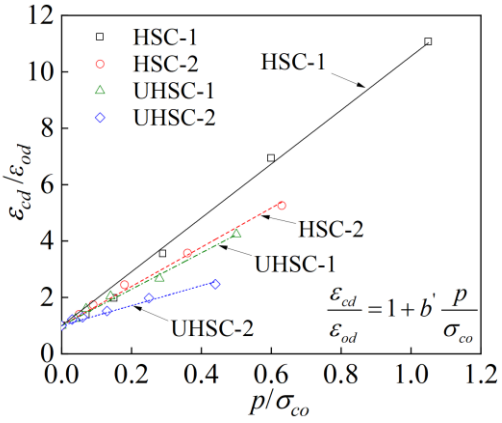

Fig. 11 – Relationship between p/σ_{co} and $\varepsilon_{cd}/\varepsilon_{od}$

where σ_{od} and ε_{od} represent the stress and axial strain of dilatancy onset under uniaxial test, σ_{cd} and ε_{cd} are the stress and axial strain of dilatancy onset under triaxial test, respectively. The test data are fitted with Eqs. (3) and (4), respectively, and the fitting curves obtained are also shown in Figures 10 and 11. The values of parameters k' and b' are shown in Table 5.

Tab.5 - The fitting parameter values for curves in Figures 10 and 11

Type	HSC-1		HSC-2		UHSC-1		UHSC-2	
Parameters	k'	b'	k'	b'	k'	b'	k'	b'
Value	21.69	9.55	18.81	6.95	16.64	6.45	12.60	3.54
R^2	0.98	0.97	0.99	0.99	0.98	0.97	0.98	0.97

$$\frac{\sigma_{cd}}{\sigma_{od}} = \sqrt{1 + k' \frac{p}{\sigma_{c_o}}} \quad (3)$$

$$\frac{\varepsilon_{cd}}{\varepsilon_{co}} = 1 + b' \frac{p}{\sigma_{co}} \quad (4)$$

Similar to the variation law between peak stress, corresponding strain at peak stress and confining pressure, the stress and axial strain of dilatancy onset of four kinds of concrete increase gradually as the confining pressure rises. The stress of dilatancy onset increases nonlinearly as the confining pressure rises, while the axial strain of dilatancy onset increases approximately linearly, which also indicates that the enhancement of the confining pressure on the stress and the strain of dilatancy onset in a negative relation to the uniaxial strength.

Volumetric model of concrete

Figure 12 shows the curves of volumetric strain versus axial strain of four kinds of concrete under different confining pressures.

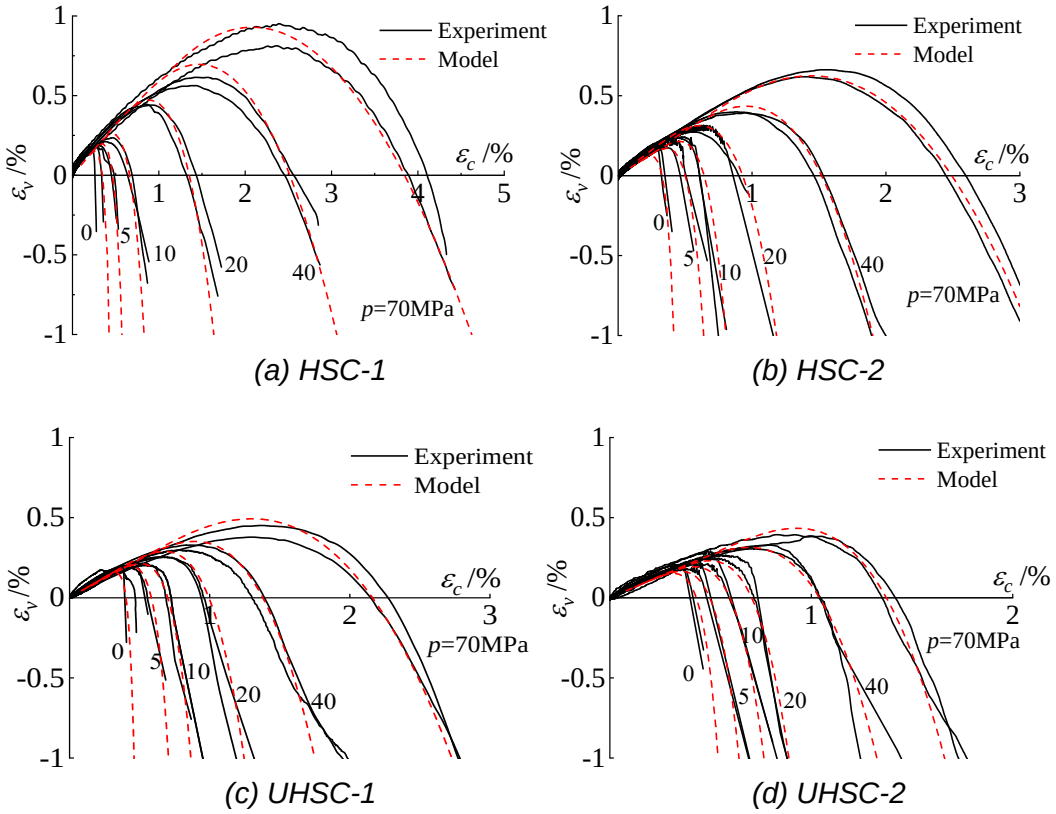

(a) HSC-1 (b) HSC-2

(c) UHSC-1 (d) UHSC-2

Fig.12 – Comparison of experimental and model values of volumetric strain

From Figure 12, it can be found that the volumetric strain increases first and then decreases as the axial strain increases. For the same types of concrete, the peak volumetric strain gradually mounts with the increase in confining pressure. For the different types of concrete, the peak volumetric strain of relatively low-strength concrete is higher than the relatively high-strength concrete under the same confining pressure.

Concrete exhibits lateral dilation or expansion behavior due to the Poisson effect under the axial pressure. Many scholars have established mathematical models to describe the expansion behavior of normal concrete under uniaxial compression according to the relationship between axial deformation and lateral deformation [21-23]. Imran and Pantazopoulou [24] proposed the concept of volumetric strain when describing this behavior, and established a mathematical model of the relationship between volumetric strain and axial strain of normal concrete under uniaxial compression. At the condition of triaxial compression, confining pressure can inhibit the initiation and

propagation of cracks in concrete, which has a greater impact on the change of volume of concrete. Based on the original model, Sheikh [25] proposed the volumetric model of normal and high-strength concrete under triaxial compression. This model assumes that the volumetric strain of concrete in the initial stage of compression increases approximately linearly with the increase of axial strain and changes in a parabolic shape after the concrete cracks. The general form of the model under triaxial compression can be express as follows:

$$\varepsilon_v = (1-2v)\left[\frac{2p}{E_c} + \varepsilon_c^{vo}\left(\frac{\varepsilon_c}{\varepsilon_c^{vo}} - d\left[\frac{\langle \varepsilon_c - \varepsilon_c^{\lim}\rangle}{\varepsilon_c^{vo} - \varepsilon_c^{\lim}}\right]^e\right)\right] \quad (5)$$

where v is Poisson's ratio, and ε_{vo} crepresents the axial strain corresponding to zero volumetric strain, its value is related to ε_{cc} and can be expressed as $\varepsilon_c^{vo} = m\varepsilon_{cc}$, the value of parameter m mainly depends on the uniaxial compressive strength of concrete. The expression of m given in [25] is as follows:

$$0.65 \le m = \frac{\sigma_{co}}{\langle \sigma_{co} - 50\rangle + 40} - 0.1 \le 1.1 \quad (6)$$

$\varepsilon_c^{\lim}$ in Eq. (5) is the axial strain corresponding to concrete cracking in the lateral direction and can be expressed as:

$$\varepsilon_c^{\lim} = \frac{1-v}{vE_c}p - \frac{\varepsilon_{cr}}{v} \quad (7)$$

where ε_{cr} can be calculated from the splitting strength σcr and determined by the expression in [25]:

$$\varepsilon_{cr} = \frac{\sigma_{cr}}{E_c} = \frac{0.387\sigma_{co}^{0.63}}{E_c} \quad (8)$$

The McCauley brackets⟨ ⟩in Eqs. (5) and (6) are defined as$\langle x\rangle = 0.5[x + \text{abs}(x)]$. Through observation and analysis, it can be known that the values of parameters d and e are mainly controlled by the shape of the ε_v-ε_c curve. The value of parameter d increases as the confining pressure level mounts, which controls the size of shape of the curve, while the value of parameter e decreases with the increase in confining pressure level, which is related to the steepness of the peak of the curve. The parameters d and e in Eq. (5) are defined in [25], and the expressions are given as follows:

$$d = 1 - \frac{p}{\sigma_{co}} \ge 0.7 \quad (9)$$

$$e = \frac{\sigma_{co} - p}{30} \ge 2.0 \quad (10)$$

It can be seen from Eqs. (9) and (10) that they are only applicable to the conditions where the confining pressure level p/σ_{co} ≤ 0.3and the difference between strength and confining pressure is greater than 60MPa. Therefore, expressions of d and e were improved in this paper, which can satisfy a wider range of confining pressure levels:

$$d = \sqrt{\frac{p/\sigma_{co} + 0.11}{0.8}} \quad (11)$$

$$e = \frac{2.23}{d} \quad (12)$$

In this paper, the value ranges of the two parameters were $0.34 \le d \le 1.21$ and $1.84 \le e \le 6.56$, respectively. Figure 12 shows the comparison between the experimental curves and predicted curves obtained by the model of volumetric strain versus axial strain. The comparison shows relatively good agreement between experimental and predicted results, which indicates that the improved model can better describe the variation law of volumetric strain of concrete with confining pressure level range of 0-1.05 and strength range of 67 MPa-160 MPa.

FAILURE CRITERIONS

Mohr-Coulomb criterion

The Mohr-Coulomb criterion postulates that under normal stress on a certain plane inside the material, when the shear stress reaches its ultimate shear strength, the material will be failure. The theory describes the failure behavior of the material under the combined action of normal stress and shear stress. This failure criterion can be expressed by the failure envelope determined by Mohr's circle under different stress states in τ-σ coordinate system. Based on the uniaxial and triaxial compression test data, a series of Mohr circles of concrete under different stress states can be drawn in the τ-σ coordinate system, and the failure envelopes of Mohr circles of four kinds of concrete under different confining pressures can be obtained, as shown in Figure 13.

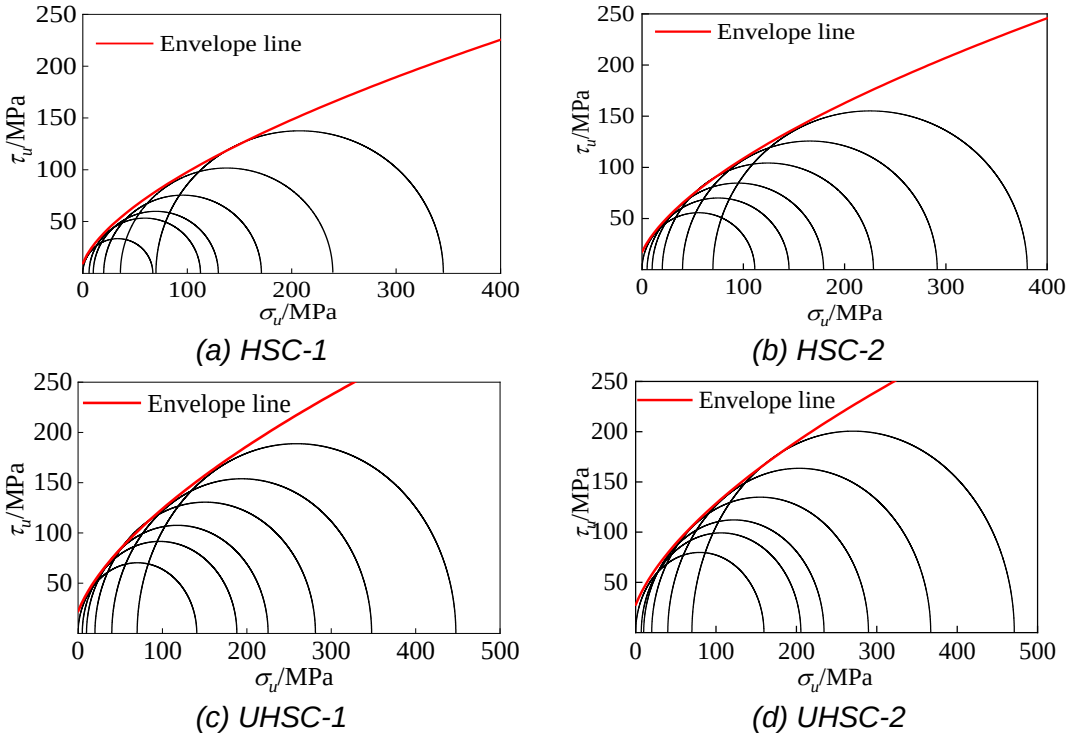

(a) HSC-1 *(b) HSC-2*

(c) UHSC-1 *(d) UHSC-2*

Fig.13 – Failure envelopes of four kinds of concrete

The power function form of the failure envelope can be obtained by nonlinear regression fitting analysis:

$$\tau_u = k(c + \sigma_u)^n \tag{13}$$

where c is the parameter about the cohesion of concrete, the value of the cohesion is shear stress kc^n at the intersection of envelope and longitudinal axis. k and n are the test fitting parameters.

Table 6 shows the values of the parameters in the Eq. (13). The cohesion of concrete gradually increases as the uniaxial compressive strength rises, which is due to the decrease of water/cement ratio and the improvement of concrete shear strength. Moreover, significant improvements in the interface between mortar and aggregate are contributed by the addition of silica fume to ultra-high-strength concrete.

Tab.6 - Fitted values of parameters in the expression

Parameters	HSC-1	HSC-2	HSCU-1	UHSC-2
k	5.812	6.539	7.152	7.793
c	2.425	5.144	6.326	8.363
n	0.609	0.605	0.612	0.598
R^2	0.9936	0.9978	0.9954	0.9982

The values of the shear stress and normal stress for the four kinds of concrete are normalized by the corresponding value of the uniaxial compressive strength, respectively. The relationship curve between the τ_u/σ_{co} and σ_u/σ_{co} is shown in Figure 14, and the general nonlinear formula of the failure envelopes was obtained:

$$\frac{\tau_u}{\sigma_{co}} = \alpha(\beta + \frac{\sigma_u}{\sigma_{co}})^s \quad (14)$$

where α =1.035, β =0.047, s=0.629. Figure 14 shows the comparison between the fitting curve and experimental data. It can be seen that the general nonlinear expression of the Mohr-Coulomb failure criterion can more accurately describe the failure envelopes of four kinds of concrete.

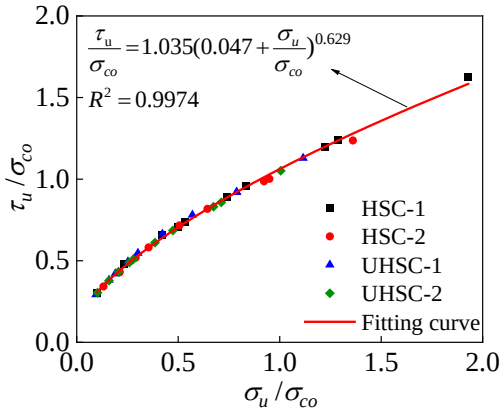

Fig.14 – Normalized failure curve for Mohr-Coulomb failure criterion

CONCLUSION

This study investigated the mechanical properties of four types of concrete with uniaxial strengths of 67.01, 109.34, 140.65, and 159.61 MPa containing the same basalt coarse aggregate under uniaxial compression test and conventional triaxial compression test. The volumetric deformation patterns and damage modes of the specimens were analysed, and the damage envelopes were obtained by using the nonlinear Mohr-Coulomb criterion, which was used to describe the mechanical properties of concrete under triaxial stress. From these investigations and test results, following conclusions can be drawn.

1) Different compressive strengths of concrete will influence its failure modes due to the difference in physical and mechanical characteristics between mortar and coarse aggregate. In uniaxial compressive test, the failure modes of different concretes types are all vertical split failure. As the confining pressure increases, the failure modes of concrete all develop from oblique shear failure toward extrusion flow failure. Crack propagation paths and morphologies in high-strength concrete, however, are different from those in ultra-high-strength concrete. In high-strength concrete, the cracks bypass the aggregate to propagate, and the failure mainly occurs in the matrix mortar or the interface between matrix mortar and aggregate, while in ultra-high-strength concrete, the crack pass through the coarse aggregates when expanding to the aggregates, the percentage of cracks

bypassing the aggregate decreased from 85.7% to 32.4% as the strength increased, the failure is mainly caused by the joint damage of mortar matrix and aggregate.

2) The enhancement of the confining pressure on the peak stress and stress of dilatancy onset, the corresponding strain at the point of peak stress and dilatancy onset of four concrete all in negative relation to its uniaxial compressive strength.

3) Confining pressure has a significant effect on the behavior of expansion and failure of concrete. Under the condition of low confining pressure, the difference between the peak stress and the stress of dilatancy onset, and the difference between the strain at peak stress and dilatancy onset are both really minimal, which indicates that the concrete will be broken rapidly after the dilatancy behavior occurs, while the difference increase gradually with the increase in confining pressure, indicating the failure of concrete are delayed by confining pressure.

4) The confining pressure can markedly increase the peak volumetric strain of concrete. At the condition of same confining pressure, the peak volumetric strain of concrete with relatively low uniaxial compressive strength is greater than the relatively uniaxial compressive strength. Based on the test results, the parameters in the existing volumetric model of concrete are improved, which makes the model predict the change of the volumetric strain of high-strength and ultra-high-strength concrete in a larger confining pressure range.

5) Based on the experimental data, the failure envelopes of four kinds of concrete under uniaxial and triaxial stress state were obtained by using the nonlinear Mohr-Coulomb criterion. The failure criteria can better describe the multiaxial mechanical behaviour of high-strength and ultra-high-strength concrete.

The results and research methodology of this paper can provide theoretical support when utilizing basalt in the formulation of concrete when studying the mixing ratios of concrete of different strengths.

REFERENCES

[1] Richart, FE., Brandtzaeg, A., Brown, RL., 1928. A study of the failure of concrete under combined compressive stresses. Bulletin No. 185. Engineering Experiment Station, Vol. 26, No. 12.

[2] Chinn, J., Zimmerman, RM., 1965. Behavior of plain concrete under various high triaxial compression loading conditions. Technical Report; No. WL TR64-163(AD468460), Air Force Weapons Laboratory, New Mexico.

[3] Mills, LL., Zimmerman, RM., 1970. Compressive strength of plain concrete under multiaxial loading conditions. Journal of the American Concrete Institute, Vol. 66: 802-807. https://doi.org/10.14359 /7310

[4] Launay, P., Gachon, H., Kesler, CE., 1972. Strain and ultimate strength of concrete under triaxial stress. ACI SP Concrete for Nuclear Reactors, Vol. 34: 269–282. https://doi.org/10.1590/S1413-24782006000200012

[5] Sfer, D., Carol, I., Gettu, R., Etse G., 2002. Study of the behavior of concrete under triaxial compression. Journal of Engineering Mechanics, Vol. 128, No. 2: 156-163. https://doi.org/10.1061/(ASCE) 0733-9399(2002) 128:2(156

[6] Xie, J., Elwi, AE., Macgregor, JG., 1995. Mechanical properties of three high-strength concretes containing silica fume. ACI Materials Journal, Vol. 92, No. 2: 135-145. https://doi.org/10.14359 /9764

[7] Song, YP., 2008. Failure mode and constitutive model of plain high-strength high-performance concrete under biaxial compression after exposure to high temperatures. Acta Mechanica Solida Sinica, Vol. 21, No. 02: 149-159. https://doi.org/10.1007/s10338-008-0818-1

[8] He, ZJ., Song, YP., 2010. Multiaxial tensile–compressive strengths and failure criterion of plain high-performance concrete before and after high temperatures. Construction and Building Materials, Vol. 24, No. 4: 498-504. https://doi.org/10.1016/j.conbuildmat. 2009.10.012

[9] Ansari, F., Li, QB., 1998. High-strength concrete subjected to triaxial compression. ACI Materials Journal, Vol. 95, No. 6: 747-755. https://doi.org/10.14359/420

[10] Ma, J., Orgass, M., Dehn, F., Schmidt, D., Tue, NV., 2004. Comparative investigations on ultra-high-performance concrete with and without coarse aggregates. In: Proceedings of the 1st International Symposium on Ultra-High-Performance Concrete, 205-212. Kassel University Press, Kassel, Germany.
[11] Graybeal, BA., 2007. Compressive behavior of ultra-high-performance fiber-reinforced concrete. ACI Materials Journal, Vol. 104, No. 2: 146-152. https://doi.org/10.14359/18577
[12] Graybeal, BA., Baby, F., 2013. Development of direct tension test method for ultra-high-performance fiber-reinforced concrete. ACI Materials Journal, Vol. 110, No. 2: 177-186. https://doi.org/10.14359/51685532
[13] Leutbecher, T., Fehling, E., 2004. Structural behavior of UHPC under tensile stress and biaxial loading. In: Proceedings of the International Symposium on Ultra High-Performance Concrete, 435-446, Kassel University Press, Kassel, Germany.
[14] Curbach, M., Speck, K., 2008. Ultra high-performance concrete under biaxial compression. In: Proceedings of the Second International Symposium on Ultra High-Performance Concrete, 477-484, Kassel University Press, Kassel, Germany.
[15] Wang, YZ., Wang, YB., Zhao, YZ., Li, GQ.， Li, H., 2020. Experimental study on ultra-high-performance concrete under triaxial compression. Construction and Building Materials, Vol. 263, No. 10. https://doi.org/10.1016/j.conbuildmat.2020.120225
[16] Zhou, XG., Wang, Z., 2019. Effect of confinement and coarse aggregate on compressive properties of ultra-high strength concrete. Journal of Harbin Institute of Technology, Vol. 51, No. 12: 144-152. https://doi.org/10.11918/j.issn.0367-6234.201903070 (in Chinese).
[17] Liew, J., Xiong, DX., 2012. Ultra-high strength concrete filled composite columns for multi-storey building construction. Advances in Structural Engineering, Vol. 15, No. 9: 1487-1504. https://doi.org/10.1260/1369-4332.15.9.1487
[18] Wang, YB., Liew, JY., Lee, SC., Xiong, DX., 2016. Experimental study of ultra-high strength concrete under triaxial Compression. ACI Materials Journal, Vol. 113, No. 1: 105-112. https://doi.org/10.14359/51688071
[19] Alexander, MG., Mindess, S., 2010. Aggregates in concrete. Taylor and Francis, New York.
[20] Farnam, Y., Moosavi, M., Shekarchi, M., Babanajad, SK., Bagherzadeh, A., 2010. Behaviour of slurry infiltrated fibre concrete (SIFCON) under triaxial compression. Cement and Concrete Research, Vol. 40, No. 11: 1571-1581. https://doi.org/10.1016/j.cemconres. 2010.06.009
[21] Chen, WF., 1988. Evaluation of plasticity-based constitutive models for concrete material. Solid Mechanica Arch, Vol. 13, No. 1: 1-63.
[22] Vecchio, FJ., 1992. Finite element modeling of concrete expansion and confinement. Journal of Structural Engineering, Vol. 118, No. 9: 2390-2406. https://doi.org/10.1061/(ASCE)0733-9445(1992)118:9(2390
[23] Cui, C., Sheikh, SA., 2010. Analytical model for circular normal- and high-strength concrete columns confined with FRP. Journal of Composites for Construction, Vol. 14, No. 5, 562–572. https://doi.org/ 10.1061/(ASCE)CC.1943-5614.0000115
[24] Imran, I., Pantazopoulou, SJ., 1996. Experimental study of plain concrete under triaxial stress. ACI Materials Journal, Vol. 93, No. 6: 589-601. https://doi.org/10.14359/9865
[25] Sheikh, SA., Laine, D., Cui, C., 2013. Behavior of normal- and high-strength confined concrete. ACI Structural Journal, Vol. 110, No. 6: 989-999. https://doi.org/10.14359/51686154